



CrossMark
click for updates

Cite this: *RSC Adv.*, 2015, 5, 64534

Received 20th May 2015
Accepted 23rd July 2015

DOI: 10.1039/c5ra09492e

www.rsc.org/advances

Green synthesis of PdCu supported on graphene/polyoxometalate LBL films for high-performance formic acid oxidation†

Ai Ma,^a Xiaofeng Zhang,^a Xiaoying Wang,^a Lijuan Le^a and Shen Lin^{*ab}

PdCu alloy nanoparticles (with sizes of ca. 4.5 nm) have been synthesized by a one-step electrochemical process on composite films constructed from functionalized graphene (GN) and H₃PMo₁₂O₄₀ (PMo₁₂) by LBL assembly. The as-prepared hybrid displays enhanced electrocatalytic activity and extended durability towards formic acid oxidation in an acid media.

Direct formic acid fuel cells (DFAFCs) which possess lots of advantages have attracted considerable attention. Formic acid as an energy carrier is easier to store and transport than hydrogen. Meanwhile, formic acid has a reduced toxicity, higher energy densities and lower fuel crossover through Nafion membranes in comparison to methanol.¹ Initial catalysis research on the DFAFCs was dominated by studies of Pt-based catalysts as anode catalysts.² In view of the catalytic efficiency, recent interests focus on Pd-based catalysts which are advantageous towards formic acid electrochemical oxidation mostly through the direct pathway.³ However, pure Pd suffers from the catalyst poisoning during the formic acid electro-oxidation reaction more or less.⁴ In order to further improve the catalytic activity and stability while lower the overall cost of anode catalyst, Pd is used to combined with a transition metal (such as Cu, Co, Ni, Fe, Ir, *etc.*) to form the binary alloy.⁵ The enhancement is mainly due to the formation of bimetallic interaction which is stronger than a single metal–oxygen (M–O) interaction so as to weak the adsorption of inhibiting reaction intermediates (*i.e.* CO_{ads}) on catalyst surface,⁶ which has been explained by the electronic, strain, or alloying effects.⁷

Graphene (GN) could be a desirable support substrate for growing and anchoring metal NPs due to its large surface area, excellent conductivity, chemical stability, mechanical strength

and light weight.⁸ On other hand, polyoxometalates possess metal–oxygen frameworks and undergo reversible and stepwise, multi-electron-transfer reactions. Their rich redox property has made them attractive candidates for electrode modification, electrocatalysis, and electroanalysis.⁹

In this study, first, PDDA-GN/PMo₁₂ films were prepared by layer-by-layer electrostatic assembly as supports: on one hand, poly (diallyldimethylammonium chloride) (PDDA) has excellent binding capability with graphene so as to increase the solubility and decrease agglomeration of graphene and could maintain the electronic structure of graphene;¹⁰ on the other hand, phosphomolybdic acid (PMo₁₂) with strong oxidation ability can more easily convert CO_{ads} to CO₂ releasing the active sites of catalysts for further electrochemical reaction. Furthermore, LBL assembly is an advisable method for the deposition of inorganic–organic hybrid thin films owing to the merits such as low cost, room temperature process, and especially the controllable thickness at a molecular scale.¹¹ PdCu alloy is very fascinating for its high catalytic performance and founded to exhibit strong synergy for the formic acid electro-oxidation.¹² We perform an electrochemical synthesis experiment to allow the formation of PdCu nanoparticles at room temperature, in a green, facile and efficient way (see experimental details in ESI†). In addition, the produced PdCu@PDDA-GN/PMo₁₂ catalyst, as a continuation of our previous research,¹³ is used as an anode and tested in formic acid oxidation. We put forth effort to discuss the three components of PDDA-GN, PMo₁₂ and binary alloy PdCu play the roles respectively, and how a synergistic effect can dramatically improve the stability the electrocatalytic activity of the Pd-based catalyst regarding formic acid oxidation.

Fig. 1a shows a TEM image of PdCu@PDDA-GN/PMo₁₂ containing small homogeneous particles in nanometric size with spherical morphology on the thin films. In the absence of PdCu with other conditions unchanged, the as-produced sample is PDDA-GN/PMo₁₂. We also observed the morphology and thickness of PDDA-GN/PMo₁₂ films through FE-SEM and AFM (ESI, Fig. S1a and S2†). The histogram (the inset of Fig. 1a) indicates a particle size distribution with values ranging from 2

^aCollege of Chemistry & Chemical Engineering, Fujian Normal University, Fuzhou 350007, China. E-mail: shenlin@fjnu.edu.cn; Fax: +86-591-22867399; Tel: +86-591-22867399

^bFujian Key Laboratory of Polymer Materials, Fuzhou 350007, Fujian, China

† Electronic supplementary information (ESI) available. See DOI: 10.1039/c5ra09492e

to 5.5 nm. The distinct lattice fringes of $d = 0.218$ nm match with the crystallographic plane of PdCu (111) which indicate the existence of the single-phase PdCu alloy.¹⁴ SAED pattern (the inset of Fig. 1b) is also providing quick and easy crystal orientation information of the obtained PdCu. The lattice spacing measured from the diffraction rings of PdCu was matched well for JCPDS: 48-1551 data, which demonstrated that the PdCu have good face-centered crystalline structure.

EDS (Fig. 2a) indicates that the as-prepared PdCu alloy is composed of Pd and Cu with an atomic ratio of 1:1.5. The X-ray diffraction patterns of the blank ITO (curve a) and PdCu@PDDA/GN on ITO (curve b) are shown in Fig. 2b. The 2θ values corresponding to the (222), (400), (440) and (622) crystal face diffraction peaks for ITO are 30.6° , 35.6° , 50.8° and 60.5° , respectively.¹⁵ The graphene and PMo_{12} are absent in the XRD because their contents are low and PMo_{12} clusters do not exist in the crystalline state, but in the dispersed state. As illustrated in pattern b, the diffraction pattern shows no diffraction peaks match to Pd or Cu reported on standard JCPDS cards (Pd, 65-2867), (Cu, 04-0836), respectively. However, it is easy to find one peak at about 41° besides the peaks for ITO, which can be assigned to the diffraction peaks from the (111) crystal face of the face-centered cubic lattice PdCu alloy.⁶ This indicates the formation of the single-phase PdCu alloy which is agree with results obtained from data of Fig. 1b. From the full width half maximum of the (111) peak, the volume-averaged particles size is estimated by the Scherrer's equation: $D = 0.89\lambda_{\text{Cu}\alpha} / B_{2\theta} \cos \theta_{\text{max}}$, where D is the mean size of the PdCu particles, $\lambda_{\text{Cu}\alpha}$ is the X-ray wave-length (Cu $\text{K}\alpha$ $\lambda_{\text{Cu}\alpha} = 1.54056 \text{ \AA}$), θ_{max} is the maximum angle of the (111) peak, and $B_{2\theta}$ is the half-peak width for PdCu (111) in radians. The mean PdCu particle size of is 4.5 nm, which is consistent with the histogram obtained from TEM.

The XPS full spectrum on the PdCu@PDDA-GN/ PMo_{12} (Fig. 3a) is mainly dominated by the signals of Pd3d, Cu2p, C1s and O1s elements, respectively. Meanwhile, we can also find weak signals of P2p, Mo3d and N1s, indicating there are small amounts of PMo_{12} and PDDA-GN. Besides XPS, we used CV to detect PMo_{12} and the number of film layers (ESI, Fig. S3†). The XPS spectra of C1s in Fig. 3b correspond to PDDA-GN species. The C–O peak intensities significantly decrease, which indicates that the percentage of surface oxygen groups in PDDA-GN is

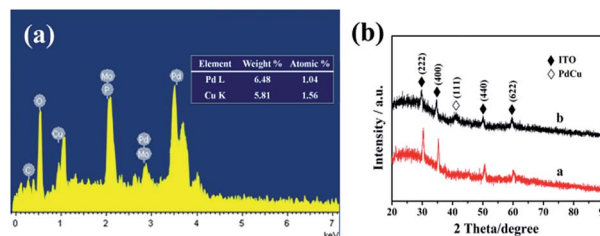


Fig. 2 (a) EDS spectrum of the PdCu@PDDA-GN/ PMo_{12} . (b) XRD patterns of the blank ITO (curve a) and the PdCu@PDDA-GN/ PMo_{12} on an ITO electrode (curve b).

reduced obviously after treatment with hydrazine in the presence of PDDA. These results imply that considerable deoxygenation occurred by PDDA grafting and hydrazine reduction. The Cu2p peaks appeared at 933.1 eV and 952.9 eV were observed from Fig. 3c, which were attributed to the $\text{Cu}2p_{3/2}$ and $\text{Cu}2p_{1/2}$ bands, respectively. Two peaks (Fig. 3d) at 335.1 eV and 340.4 eV in the Pd3d region corresponded to $\text{Pd}3d_{5/2}$ and $\text{Pd}3d_{3/2}$ bands, respectively. These peaks demonstrated the Cu and Pd on the surface of catalyst. Compared to the standard zero-valent copper and palladium binding energy (ESI, Table S2†),¹⁶ $\text{Cu}2p_{3/2}$ and $\text{Cu}2p_{1/2}$ shifted to higher binding energy (shifted by 0.6 eV and 0.3 eV) while $\text{Pd}3d_{5/2}$ and $\text{Pd}3d_{3/2}$ binding energy shifted to lower (shifted by 0.3 eV and 0.4 eV), which due to electron interaction between Cu and Pd atomic orbital.¹⁷ This result implied further that PdCu alloy had formed.

The electrochemically active surface area (ECSA) of the catalysts modified electrodes was determined by CO-stripping cyclic voltammetry (Fig. 4a). The associated ECSA (ESI, Table S1†) was obtained from the following equation:¹⁷ $\text{ECSA} = Q/M \times 420$, where Q is the charge of CO desorption-electrooxidation in micro-coulomb (μC), M represents the total amount of Pd (μg) on the electrode surface, and $420 \mu\text{C cm}^{-2}$ is the charge required to oxidize a monolayer of CO on the Pd catalyst. The ECSA is estimated to be $23.62 \text{ m}^2 \text{ g}^{-1}$ Pd for the PdCu@PDDA-GN/ PMo_{12} (Fig. 4a), which is about 2.3 times of commercial Pd/C ($10.33 \text{ m}^2 \text{ g}^{-1}$ Pd). The enlarged ECSA is ascribed to the

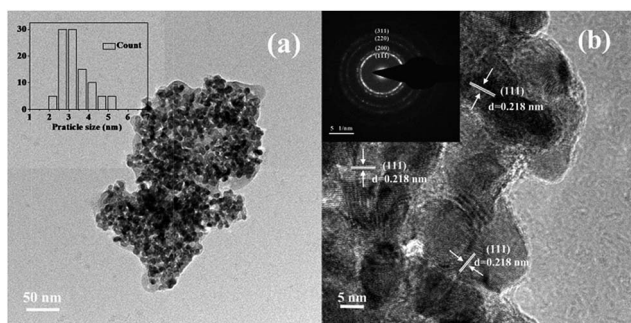


Fig. 1 (a and b) TEM and HRTEM images of the PdCu@PDDA-GN/ PMo_{12} . Insets show the corresponding size distribution in image (a) and SAED pattern in image (b).

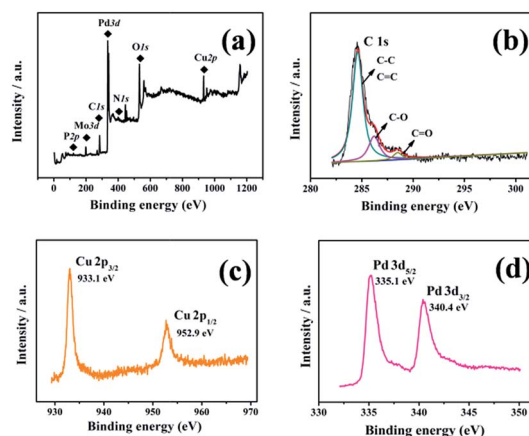


Fig. 3 XPS spectra of full spectrum (a), C1s (b), Cu2p (c), and Pd3d (d) of the PdCu@PDDA-GN/ PMo_{12} on an ITO electrode.

homogeneous distribution of the PdCu nanoparticles on films of PDDA-GN/PMo₁₂. The onset potential of CO-stripping negatively shifts 110 mV on the PdCu@PDDA-GN/PMo₁₂ modified electrode, compared with the commercial Pd/C, indicating the enhanced CO tolerance ability. For one thing, the strength of Pd and Cu interactions is great strong so as to weak the adsorption of inhibiting reaction intermediates (*i.e.* CO_{ads}) on catalyst surface.¹⁸ For another, the beneficial role of HPMo₁₂ for CO further electro-oxidation and release of surface active sites by CO removal.¹⁹

The electrochemical stability of the PdCu@PDDA-GN/PMo₁₂ was also investigated in 0.5 M H₂SO₄ containing formic acid at an applied potential of 0.2 V for 3600 s (Fig. 4b). The polarization currents on the PdCu@PDDA-GN/PMo₁₂ modified electrode decrease within 1000 s and then decay quite slowly to approach a limiting current (up to 3600 s). The initial currents drop quickly for the PdCu@PDDA-GN/PMo₁₂, probably due to the formation of the intermediate species during formic acid oxidation reaction.²⁰ Moreover, the corresponding limiting currents decrease to 31.53 mA mg⁻¹ Pd up to 3600 s, which is much higher than the commercial Pd/C (15.65 mA mg⁻¹ Pd) catalysts under the same conditions. The activity results of Pd with the same conditions are also lower than PdCu@PDDA-GN/PMo₁₂ (ESI, Fig. S4[†]). The improved catalytic activity and better stability of the PdCu@PDDA-GN/PMo₁₂ was further confirmed by cyclic voltammetry. The catalytic current density keeps almost constant within 100 cycles. With the peak current density of the 5th cycle in the forward sweep as a reference, the peak current density of the PdCu@PDDA-GN/PMo₁₂ remains about 92% of its original value after 100 cycles. From Fig. 4b and c, the PdCu@PDDA-GN/PMo₁₂ is conspicuously better than commercial Pd/C at electrocatalytic activity and better stability for formic acid oxidation.

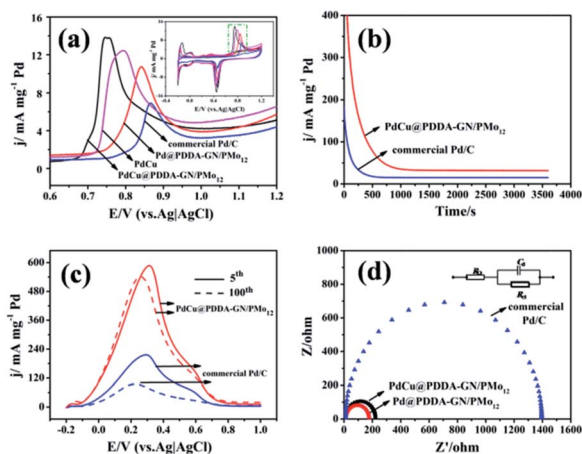


Fig. 4 (inset a) CO-stripping voltammograms and (a) magnified area enclosed by a green square of different electrocatalysts in 0.5 M H₂SO₄ solution with a scan rate of 50 mV s⁻¹. (b) Chronoamperometric curves of different electrocatalysts in 0.5 M H₂SO₄ solution containing 1 M HCOOH at 0.2 V for 3600 s. (c) Positive-going cyclic voltammograms of different electrocatalysts in 0.5 M H₂SO₄ solution containing 1 M HCOOH with a scan rate of 50 mV s⁻¹. (d) Nyquist plots of different electrocatalysts in 0.5 M H₂SO₄ solution.

In addition, the enhanced electrocatalytic performance may be owing to the superior electric conductivities of the polymer-modified graphene (PDDA-GN) in the multilayer films,²¹ which can be proven by Nyquist plots of the electrochemical impedance spectrum (EIS) (Fig. 4d). The impedance measurements were made with frequencies ranging from 0.01 Hz to 10⁵ Hz and an amplitude voltage of 0.1 V. The impedance data can be fitted by an equivalent electrical circuit composed by one series circuit of a resistance (R_{ct}) and capacitor (C_d) in parallel.²² Usually, the high-frequency semicircle diameter is equal to the charge-transfer resistance (R_{ct}), which is resulted from the charge transfer process at the interface of electrode/electrolyte.²³ As shown in Fig. 4d, R_{ct} markedly decreases with the introduction of PDDA-GN/PMo₁₂ into multilayer films. This means that polymer-modified graphene helps enhance electrons transfer obviously on the electrode interface. At the same time, with the preparation of LBL and electro-deposition, electrons transfer faster on the smooth and thin films than on the rough surface of Pd/C through dropping on an electrode.

In this work, a simple and facile approach was developed for preparation of the PdCu@PDDA-GN/PMo₁₂, with the assistance of Cu to obtain the better electrocatalytic activity and extended durability, using PDDA-GN as an electron carrier and PMo₁₂ as a promoter to convert CO_{ads} to CO₂ more simply. The as-prepared PdCu@PDDA-GN/PMo₁₂ exhibits a significant effect on the enhanced electrocatalytic activity, the improved tolerance of CO and better stability for formic acid oxidation. This work provides a promising strategy to fabricate graphene-supported and Pd-based alloy electrocatalysts for efficient fuel cell applications.

Acknowledgements

This work was financially supported by NSFC (No. 21171037).

Notes and references

- 1 G. L. Soloveichik, *Beilstein J. Nanotechnol.*, 2014, **5**, 1399.
- 2 (a) C. W. Liu, Y. C. Wei, C. C. Liu and K. W. Wang, *J. Mater. Chem.*, 2012, **22**, 4641; (b) N. Tian, Z. Y. Zhou, S. G. Sun, Y. Ding and Z. L. Wang, *Science*, 2007, **316**, 732.
- 3 R. Zhang, H. Liu, B. Wang and L. Ling, *J. Phys. Chem. C*, 2012, **116**, 22266.
- 4 J. F. Zhang, Y. Xu and B. Zhang, *Chem. Commun.*, 2014, **50**, 13451.
- 5 (a) J. W. Chen, Y. J. Li, Z. C. Gao, G. Wang, J. Tian, C. P. Jiang, S. F. Zhu and R. L. Wang, *Electrochem. Commun.*, 2013, **37**, 24; (b) S. J. Li, D. J. Cheng, X. G. Qiu and D. P. Cao, *Electrochim. Acta*, 2014, **143**, 44; (c) M. A. Matin, J. H. Jang and Y. U. Kwon, *J. Power Sources*, 2014, **262**, 356.
- 6 C. G. Hu, X. Q. Zhai, Y. Zhao, K. Bian, J. Zhang, L. T. Qu, H. M. Zhang and H. X. Luo, *Nanoscale*, 2014, **6**, 2768.
- 7 (a) C. Xu, Y. Liu, J. Wang, H. Geng and H. Qiu, *J. Power Sources*, 2012, **199**, 124; (b) A. K. Singh and Q. Xu, *ChemCatChem*, 2013, **5**, 652.
- 8 (a) Y. S. Feng, J. J. Ma, Y. M. Kang and H. J. Xu, *Tetrahedron*, 2014, **70**, 6100; (b) J. Saleem, P. Gao, J. Barford and G. Mckay,

- J. Mater. Chem. A*, 2014, **2**, 13745; (c) Z.-L. Wang, H.-L. Wang, J.-M. Yan, Y. Ping, S.-I. O, S.-J. Li and Q. Jiang, *Chem. Commun.*, 2014, **50**, 2732; (d) J.-M. Yan, Z.-L. Wang, L. Gu, S.-J. Li, H.-L. Wang, W.-T. Zheng and Q. Jiang, *Adv. Energy Mater.*, 2015, **5**, 1500107.
- 9 M. Kourasi, R. G. A. Wills, A. A. Shah and F. C. Walsh, *Electrochim. Acta*, 2014, **127**, 454.
- 10 J.-J. Shi, G.-H. Yang and J.-J. Zhu, *J. Mater. Chem.*, 2011, **21**, 7343.
- 11 Y. Xiang, S. F. Lu and S. P. Jiang, *Chem. Soc. Rev.*, 2012, **41**, 7291.
- 12 S. F. Ho, A. Mendoza-Garcia, S. J. Guo, K. He, D. Su, S. Liu, O. Metin and S. H. Sun, *Nanoscale*, 2014, **6**, 6970.
- 13 A. Ma, X. F. Zhang, Z. S. Li, X. Y. Wang, L. T. Ye and S. Lin, *J. Electrochem. Soc.*, 2014, **161**, F1224.
- 14 C. X. Xu, A. H. Liu, H. J. Qiu and Y. Q. Liu, *Electrochem. Commun.*, 2011, **13**, 766.
- 15 Z. Y. Sun, J. B. He, A. Kumbhar and J. Y. Fang, *Langmuir*, 2010, **26**, 4246.
- 16 E. B. Fox, S. Velu, M. H. Engelhard, Y.-H. Chin, J. T. Miller, J. Kropf and C. Song, *J. Catal.*, 2008, **260**, 358.
- 17 S. Z. Hu, L. Scudiero and S. Ha, *Electrochim. Acta*, 2012, **83**, 354.
- 18 S. Z. Hu, L. Scudiero and S. Ha, *Electrochem. Commun.*, 2014, **38**, 107.
- 19 L. D'Souza, M. Noeske, R. M. Richards and U. Kortz, *J. Colloid Interface Sci.*, 2013, **394**, 157.
- 20 H. Miyake, T. Okada, G. Samjeske and M. Osawa, *Phys. Chem. Chem. Phys.*, 2008, **10**, 3662.
- 21 K. P. Liu, J. J. Zhang, G. H. Yang, C. M. Wang and J. J. Zhu, *Electrochem. Commun.*, 2010, **12**, 402.
- 22 P. R. Bueno, S. A. Pianaro, E. C. Pereira, L. O. S. Bulhões, E. Longo and J. A. Varela, *J. Appl. Phys.*, 1998, **84**, 3700.
- 23 P. Joshi, L. F. Zhang, Q. L. Chen, D. Galipeau, H. Fong and Q. Q. Qiao, *ACS Appl. Mater. Interfaces*, 2010, **2**, 3572.